RESEARCH ARTICLE SUMMARY

ANTIMICROBIAL PROTEINS

The mechanism of the phage-encoded protein antibiotic from ΦX174

Anna K. Orta†, Nadia Riera†, Yancheng E. Li, Shiho Tanaka, Hyun Gi Yun, Lada Klaic, William M. Clemons Jr.*

INTRODUCTION: As part of their life cycle, viruses must escape from their hosts. For bacteriophages, this process requires breaching the bacterial cell wall and the peptidoglycan layer. Small, single-strand DNA and RNA phages have evolved single-gene lysis proteins that disrupt peptidoglycan biosynthesis and trigger cell lysis, a mechanism also used by some antibiotics. The best-studied of these is protein E from the historically important phage ΦX174, a 91–amino acid protein that contains a conserved N-terminal transmembrane helix and an extended cytoplasmic C-terminus.

RATIONALE: Mutagenesis studies have demonstrated that the protein E transmembrane domain is sufficient for lysis, with functional mutants mapping to one face of the single transmembrane helix. The strongest phenotypes were observed for conserved prolines in this domain of protein E, with one proline being essential for lysis. Wild-type protein E requires the constitutively expressed bacterial chaperone SlyD (sensitivity to lysis D), which contains a prolyl isomerase domain and a chaperone domain. Previous work had identified mutants in MraY that confer resistance to protein E–mediated lysis. MraY catalyzes the synthesis of a peptidoglycan precursor from a soluble nucleoside-sugar-peptide and a phospholipid substrate. Although many functional questions remain about MraY, here we sought to understand how a phage protein could specifically inhibit this key enzyme and what role SlyD performed in the process.

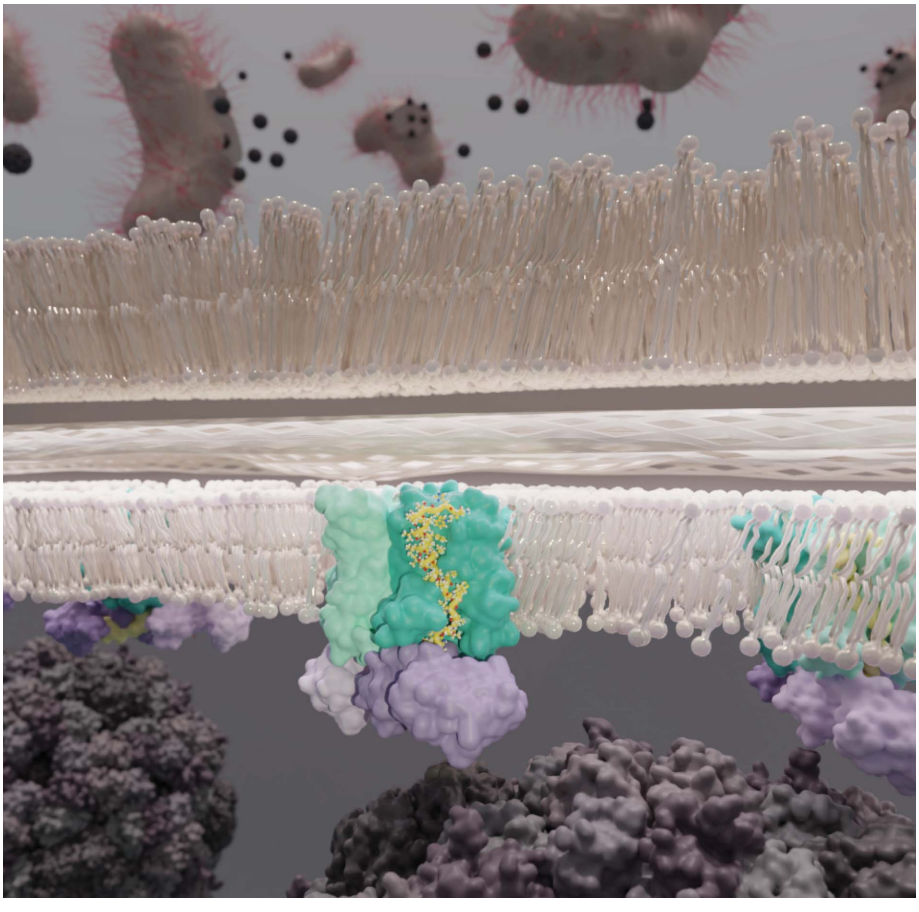

The escape of ΦX174 from its bacterial host. In the membrane is the YES complex [*E. coli* enzyme MraY (cyan), phage protein E (yellow), and *E. coli* chaperone SlyD (purple)] where protein E disrupts peptidoglycan synthesis by inhibiting MraY and allowing breaching of the cell wall (tan). Assembled ΦX174 phage particles are shown in gray. In the background are bacterial cells that are lysing at their septal division point.

RESULTS: We established that phage protein E forms a stable complex with the *Escherichia coli* proteins MraY and SlyD, designated the YES complex (MraY, protein E, SlyD). After solubilizing in detergent, we determined structures of the YES complex by single-particle electron cryo–microscopy. In our structures, the MraY dimer adopts a back-to-back orientation with the membrane-exposed active sites facing away from each other. Two SlyD molecules can be fit into the density on the cytoplasmic side. The two MraY and SlyD chains are bridged by two protein E molecules. The transmembrane helix of protein E occupies a groove on MraY corresponding to the putative binding site of the lipid substrate. At the cytoplasmic surface, the transmembrane domain of protein E bends to cross the active site, followed by an α-helix that extends to the chaperone domain of SlyD. The C-terminus of protein E continues through a peptide-binding groove in the second SlyD and into the prolyl isomerase active site. The consequence is that protein E inhibits MraY by blocking lipid access to the active site. Previous protein E mutant phenotypes are explained by the structure including the essential proline that allows for a kink in the transmembrane helix. For MraY, we can resolve the full chain including the conserved loop between TM1 and TM2. We show that the N terminus of MraY forms an α-helical stack with TM2 and identify ordered lipids on the protein surface. Finally, we provide evidence that the role of SlyD is to stabilize the complex.

CONCLUSION: Protein E directly inhibits MraY by obstructing the MraY active site in a stable complex with SlyD. This structure resolves key questions about how the model phage ΦX174 kills bacteria and escapes the cell. In the ΦX174 genome, the gene encoding for protein E is evolutionarily constrained by gene D, in which it is embedded. The YES complex provides a route for the rational design of protein E beyond this gene D restraint. Single-gene lysis proteins, like protein E, serve as useful models for the development of antibacterial therapies. ■

The list of author affiliations is available in the full article.
*Corresponding author. Email: clemons@caltech.edu
†These authors contributed equally to this work.
Cite this article as A. K. Orta *et al.*, *Science* **381**, eadg9091 (2023). DOI: 10.1126/science.adg9091

READ THE FULL ARTICLE AT
https://doi.org/10.1126/science.adg9091

RESEARCH ARTICLE

ANTIMICROBIAL PROTEINS

The mechanism of the phage-encoded protein antibiotic from ΦX174

Anna K. Orta[1]†, Nadia Riera[1]†, Yancheng E. Li[1], Shiho Tanaka[1], Hyun Gi Yun[1], Lada Klaic[1], William M. Clemons Jr.[1]*

The historically important phage ΦX174 kills its host bacteria by encoding a 91-residue protein antibiotic called protein E. Using single-particle electron cryo–microscopy, we demonstrate that protein E bridges two bacterial proteins to form the transmembrane YES complex [MraY, protein E, sensitivity to lysis D (SlyD)]. Protein E inhibits peptidoglycan biosynthesis by obstructing the MraY active site leading to loss of lipid I production. We experimentally validate this result for two different viral species, providing a clear model for bacterial lysis and unifying previous experimental data. Additionally, we characterize the *Escherichia coli* MraY structure—revealing features of this essential enzyme—and the structure of the chaperone SlyD bound to a protein. Our structures provide insights into the mechanism of phage-mediated lysis and for structure-based design of phage therapeutics.

The full realization of phage therapy as a solution to the antimicrobial resistance problem requires a fundamental understanding of the mechanisms viruses use to kill their host (*1*–*4*). Nearly 100 years ago, the first medical application of phages to treat infections used a cocktail containing the historically important phage ΦX174 (*5*). A rich source of critical discoveries in molecular biology (*6*–*9*), ΦX174 is a member of the *Bullavirinae* subfamily within *Microviridae*. It is found broadly in environments that contain coliform bacteria, such as the human gut (*10*), with *Escherichia coli* as its primary host. The 1977 publication of the ΦX174 single-stranded 5.4-kilobase DNA genome was a milestone for genomics, revealing 11 open reading frames (ORFs) (*11*). Most notable was the gene for lysis, *E*, that is embedded within the ORF of the scaffolding gene *D* (*12*). Expression of *E* alone is sufficient to kill bacteria (*13*). Although a variety of lysis mechanisms have been proposed (*14*–*16*), the most likely is that the product of *E*, protein E, disrupts peptidoglycan (PG) biosynthesis, culminating in a breach in the cell wall. In particular, protein E was demonstrated to directly inhibit the integral membrane enzyme MraY (*16*) dependent on the cytoplasmic chaperone SlyD (sensitivity to lysis D) (*17*, *18*).

Phage-derived single-gene lysis (SGL) proteins, such as protein E, trigger cell lysis by inhibiting PG biosynthesis [reviewed in (*19*)] providing a route for killing bacteria. Protein E includes a conserved N-terminal transmembrane domain (TMD), a cytoplasmic C-terminal domain with conserved positively charged residues in a predicted amphipathic helix, and an unstructured tail (Fig. 1A and fig. S1). Fusions of globular proteins to the C terminus of the TMD have demonstrated that the TMD is sufficient for lysis (*17*, *20*, *21*). Extensive mutational analysis identified key residues in protein E including the essential proline 21 (P21) (*17*, *20*–*23*). The mechanism through which SlyD and MraY work with protein E to facilitate rupture of the cell wall remains unknown. MraY, an important target for antimicrobial drug discovery [reviewed in (*24*)], catalyzes the transfer of a phospho-MurNAc-pentapeptide from "Park's nucleotide" (UDP-MurNAc-pentapeptide) onto the phosphate group of the 55 carbon polyisoprenyl-phosphate (C_{55}P) generating lipid I. X-ray crystal structures of MraY in detergent from the thermophilic Gram-negative *Aquifex aeolicus* (*Aa*MraY) (*25*, *26*) or the Gram-positive *Enterocloster bolteae* (*Eb*MraY) (*27*) revealed a conserved homodimeric structure, with ten TMDs per subunit. The structures localized the active site in a vestibule on the cytoplasmic side of a membrane-exposed cleft formed by TMDs 4, 5, and 9, which is the predicted access site for the lipid substrate (*28*). The constitutively expressed but nonessential (*29*) metallochaperone (*30*) SlyD contains two conserved core domains: an FK506-binding protein (FKBP) prolyl-isomerase domain and an insertion-in-flap (IF) domain that binds unfolded peptides by β-augmentation (*18*, *31*–*33*). The disordered SlyD C terminus (*31*), although important for metal binding, can be deleted without affecting chaperone activity (*34*).

In the present study, we resolve the mechanism of peptidoglycan biosynthesis inhibition by protein E. We determined the structure of the dimeric heterotrimer YES complex (*Ec*MraY, viral protein E, *Ec*SlyD) revealing that protein E physically blocks the lipid substrate from accessing the MraY active site. This work provides mechanistic insight into all three proteins and suggests a path toward development of antibacterial agents.

The structure of the YES complex

We used the protein E sequence from either the original phage ΦX174 or the shorter protein E isoform from phage ID21 (91 and 76 residues respectively), both from within *Bullavirinae* (Fig. 1A and fig. S1). We coexpressed an affinity-tagged protein $E_{ΦX174}$ and wild-type (WT) *Ec*MraY. After purification, a stable complex formed a single peak during size-exclusion chromatography (SEC) but resolved into four bands on a gel, two of which corresponded to the endogenous *Ec*SlyD (fig. S2A). A SlyD variant with the disordered C terminus removed rescued lysis activity in an *E. coli* Δ*slyD* strain (fig. S2, B to D) and ran as a single band on a gel (Fig. 1B) (*18*, *30*). This truncation, $SlyD_{154}$, was used for subsequent work except where noted.

The two protein E isoforms induced lysis at similar efficiencies when expressed in a WT *E. coli* strain (Fig. 1C). For purification, all three genes in the YES complex (WT *Ec*MraY, protein E, and truncated *Ec*SlyD) were recombinantly expressed together in the Δ*slyD* strain with a C-terminal affinity tag on protein E. The complex was extracted in detergent and ran as a single peak by SEC with all three proteins in an apparent stoichiometric complex (Fig. 1B). Structures for both the $YES_{ΦX174}$ and YES_{ID21} complexes were solved using single-particle electron cryo–microscopy (cryo-EM) (Fig. 1D and figs. S3 and S4). The final density maps were obtained following several rounds of data processing with heterogeneous and homogeneous refinements (figs. S3 and S4). The final overall masked resolution was 3.5 Å for the YES_{ID21} complex and 3.6 Å for the $YES_{ΦX174}$ complex (fig. S5). Statistics are provided in table S2. For both structures, the resolution was higher for regions in and adjacent to the membrane (figs. S3 and S4). We unambiguously built 90% of the protein residues in the complex. Sequence differences between the protein E variants are visible in the density (fig. S5), generally exposed on the surface of the complex. The YES_{ID21} complex is used as the reference structure, except where noted.

Within the density map, we could clearly distinguish two copies of each member of the YES complex (six separate proteins). When contoured to remove the detergent micelle, densities for 22 TMDs are clear, 20 of which are accounted for by the *Ec*MraY dimer (Fig. 1, D and E). Most of the cytoplasmic density can be accounted for by two SlyD molecules, which is the most flexible region of the complex (fig. S6D). The remaining protein density corresponds to two protein E molecules

[1]Division of Chemistry and Chemical Engineering, California Institute of Technology, Pasadena, CA 91125, USA.
*Corresponding author. Email: clemons@caltech.edu
†These authors contributed equally to this work.

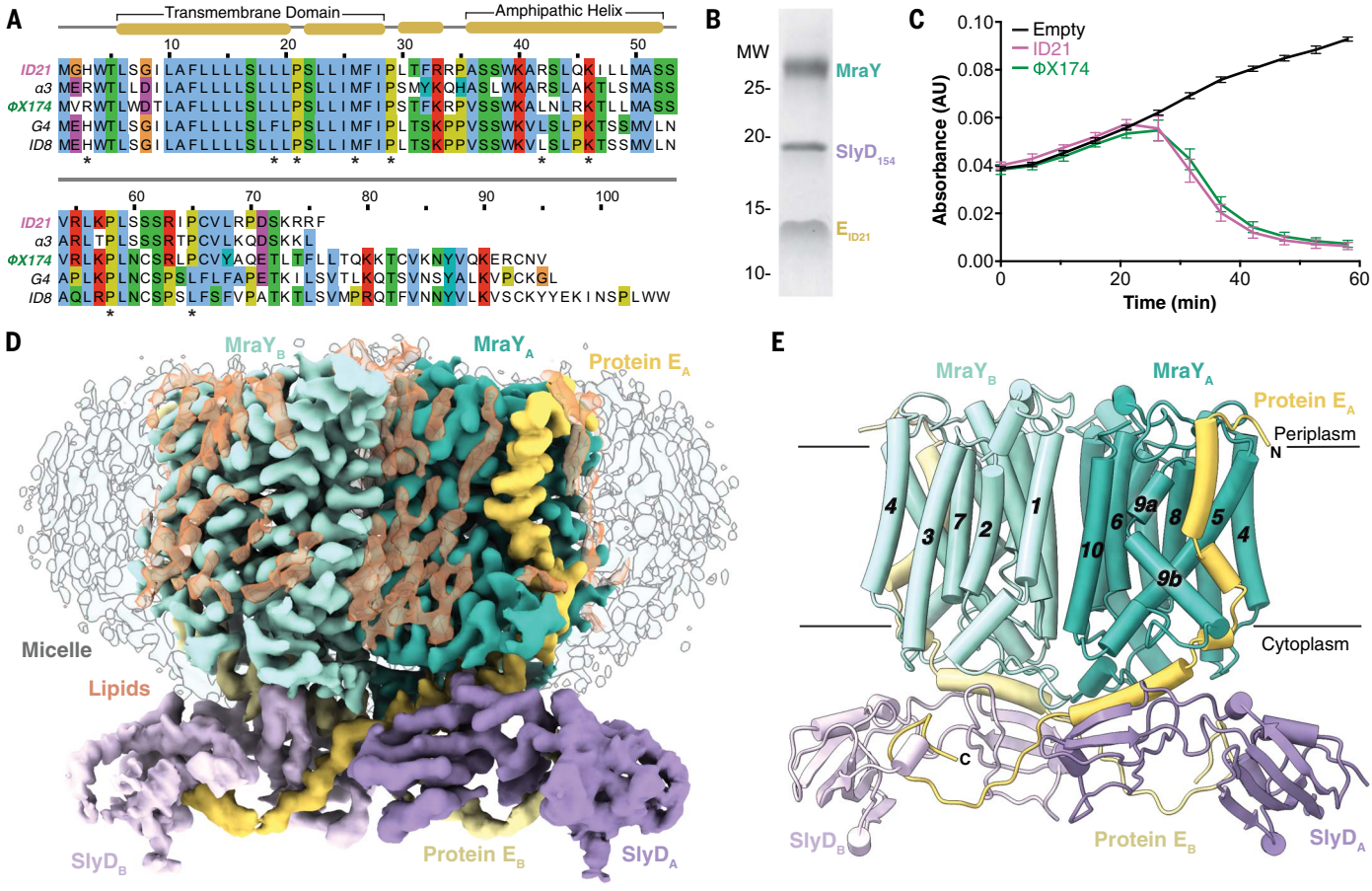

Fig. 1. The structure of the YES complex. (**A**) An alignment of a representative subset of protein E isoforms. Residue coloring is based on ClustalW. Secondary structure elements are shown above the sequence. Sequences are ordered as in fig. S1. Residues highlighted with a (*) at the bottom of the alignment are discussed in the text. (**B**) SDS-PAGE gel of the purified YES_{ID21} complex. (**C**) A lysis assay for protein E expression. Cells containing either empty vector (black line) or the protein E genes for ID21 (pink line) or ΦX174 (green line) were induced at time 0 and the absorbance at 600 nm was monitored over time. Error bars represent the standard deviation derived from $n = 3$. (**D**) Overview density maps of the YES_{ID21} complex viewed in the plane of the membrane. The detergent micelle is highlighted by gray coloration. The higher contoured map shows the six components of the twofold complex with density for *E. coli* MraY (cyan), protein E (yellow), and *E. coli* SlyD (purple) highlighted. The pairs of each protein are distinguished as the B-subunit is light purple. The general coloring scheme is maintained throughout the figures. Density that is likely lipid is shown in transparent orange. (**E**) Illustrated representation of the YES_{ID21} complex oriented and colored as in (D). Foreground TMDs for the MraYs are numbered and the bilayer is represented by lines. N terminus and C terminus of protein E_A are labeled.

that each contain a kinked TMD and a soluble domain that bridges between MraY and SlyD. Densities for lipids are visible around the membrane-exposed surface of the MraY dimer (Fig. 1D).

For protein E, starting at the N terminus in the periplasm, the TMD binds in the groove formed between TM5 and TM9 of MraY ending on the cytoplasmic side where it makes a sharp turn into the active site pocket (Figs. 1E and 2A). The TMD is followed by an amphipathic helix that crosses the active site, parallel to the membrane, presenting a positive face toward MraY and a hydrophobic face toward a SlyD IF-domain. The C-terminal residues adopt an extended conformation that primarily interacts with the second SlyD. This results in a crossover point between the two protein Es with each contacting both SlyDs. Overall, the dimeric complex (two of each of the heterotrimers) has a near twofold symmetry perpendicular to the plane of the membrane. The membrane and periplasmic facing regions overlay perfectly but the symmetry is broken at the cytoplasmic face where the C-termini of the two protein E molecules cross each other at different residues and the SlyDs adopt slightly different orientations (Fig. 1E and fig. S6). Following toward the end of protein E, we can see continuous backbone density that positions proline 65 in the active site of the FKBP domain. Beyond that, the density is insufficient to resolve the sequence and we see little difference between ΦX174 and ID21 (fig. S5).

The interaction of protein E with MraY

Functional studies have consistently revealed the requirement for a proline at position 21 (*21*, *22*, *35*). Our structure allows an elegant explanation for this requirement. The protein E TMD binds in the cleft of MraY that is defined by the angled TM9b (Fig. 2A). The proline at position 21 breaks the hydrogen bonding and introduces a kink that allows bending of the TMD around TM9b following the groove to the active site. Mutation of P21 would result in loss of the kink favoring a straight TMD that could not bind in the groove. Residue P29, also completely conserved (Fig. 1A and fig. S1), creates a second bend that completes the wrap around TM9b and a mutation at this position results in delayed lysis onset (*21*, *22*). Additional alanine mutations in the TMD identified residues that result in delayed lysis onset, postulated to decrease the binding affinity of protein E to MraY (*21*). In the present structure, most of these residues (L19, L20, L23, and M26) (Fig. 2C) make direct contact with MraY. The exception, F27, appears

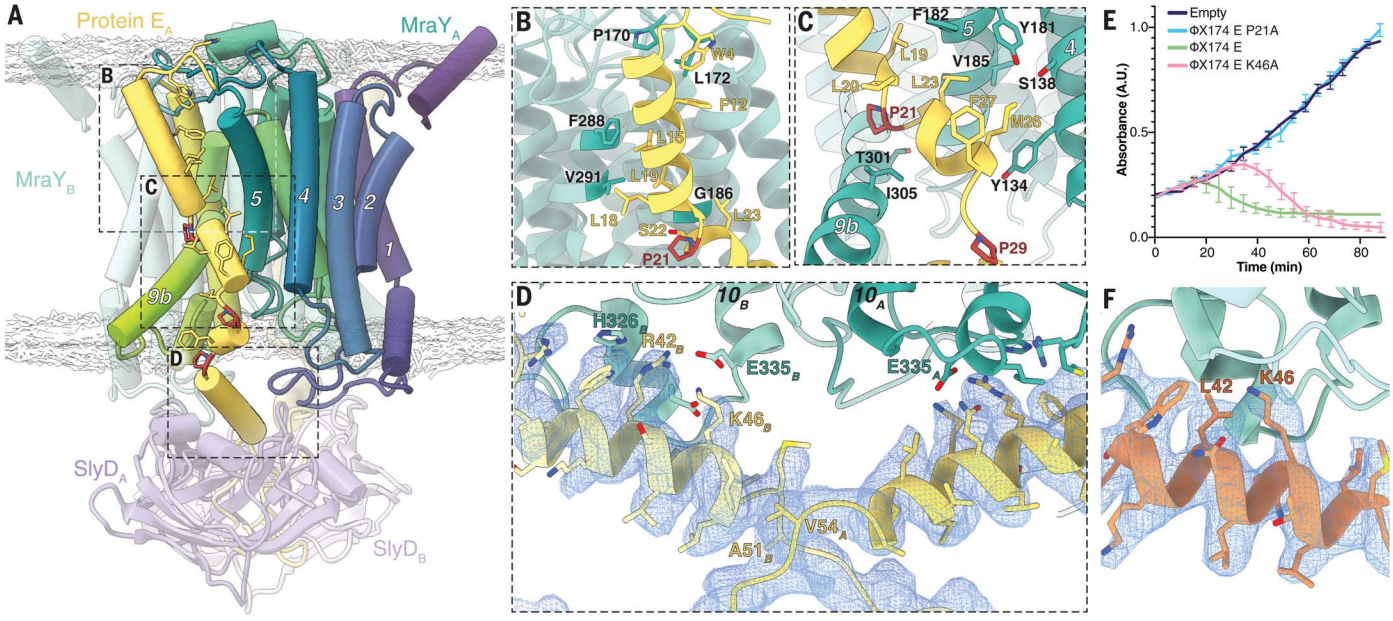

Fig. 2. The interaction of protein E with *Ec*MraY. (**A**) Illustration of the YES$_{ID21}$ complex as in Fig. 1E with a 90° rotation except that MraY$_A$ is color-ramped using the Viridis palette that goes from purple to yellow for the N- to C-terminus, respectively. Prolines are shown in red. The bilayer is modeled in white. The B-subunits and SlyDs are faded. Boxes indicate regions highlighted in panels (**B** to **D**). Side chains for protein E residues that contact MraY are shown as sticks. (B) as in (A) with positions of protein E resistance mutants in MraY highlighted (dark cyan). (C) as in (A) with residues at the interface highlighted as sticks. (D) The region where the two protein E molecules cross highlighting the asymmetry colored as in (A) with interacting residues shown as sticks. Density for the amphipathic helix of protein E shown as a blue mesh. SlyDs are removed for clarity. (**E**) Lysis assay of expressed protein E$_{\Phi X174}$ variants. Error bars represent the standard deviation derived from n = 3. (**F**) is similar to (D) for protein E$_{\Phi X174}$.

to sterically position M26 into a tight interaction with Y134 in MraY, which is conserved in most Gram-negative bacteria (fig. S7).

At the cytoplasmic interface, protein E residues A36 through M50 form the amphipathic helix spanning the width of an MraY subunit. The hydrophilic face of this helix orients toward the membrane in the MraY active site. The helix contains conserved positively charged residues that interact with conserved negatively charged residues in MraY (Fig. 2D). An example is the K46 salt bridge where, in our lysis assay, a K46A mutation resulted in delayed lysis onset (Fig. 2E). Here, isoform differences can be visualized. For example, position 42 is a leucine in ΦX174 whereas in ID21 it is an arginine that forms a salt bridge with E335 in MraY (Fig. 1). The helix ends at the crossover between the two protein Es at residue V54 in protein E$_A$ and A51 in protein E$_B$ resulting in differing interactions with residues in MraY, such as the essential H326 (Fig. 2D).

The Epos (plaques on Δ*slyD*) mutations, R3H and L19F, allow phage propagation in a Δ*slyD* background (*23*). The R3H mutant of protein E in ΦX174 results in a silent mutation in protein D and is found native to other species such as ID21 (fig. S8). Previous work reported that this variant resulted in higher levels of protein E in the membrane (*23*). In the present structure (fig. S5, G and H), this residue does not make specific contact with MraY. It is likely that the loss of a positive charge in the periplasm favors a higher percentage of protein E molecules that are correctly inserted in the membrane as a result of the positive-inside rule. L19F does not result in higher levels of protein E (*21*) and likely hastens lysis onset by having a higher affinity to MraY. Another phenylalanine mutation at the interface, L23F, also hastens lysis onset likely by higher affinity, although this is not a general rule as other leucine to phenylalanine mutants did not affect lysis (*21*). Both L19 and L23 are near the conserved F182 in MraY and may add additional stability through aromatic π interactions (Fig. 2C). The opposite mutation, phenylalanine to leucine, can show loss of binding. For example, the F288L mutation in MraY (*16*) is located at the interface with protein E and results in a loss of lysis, most likely due to lower affinity.

All the mutations in MraY that allow resistance to protein E–mediated lysis (P170L, ΔL172, G186S, F288L, V291M) (*16*, *35*) are at the interface with protein E (Fig. 2B). The mutant F288L, as noted above, lowers affinity to protein E. Residue G186 is at the nearest approach between the two proteins and a mutation to serine would prevent protein E binding. The mutant V291M lies directly at the interface near L19 in protein E, although a specific effect for this mutation is not clear. Finally, P170L and ΔL172 are located within periplasmic loop 4-5, which interacts with the conserved N terminus of protein E. Although more resistant to lysis, these two mutants are predicted to still bind protein E, albeit with lower affinity (*35*).

The mechanism of inhibition of MraY by protein E

The YES complex structure allows us to propose a simple mechanism for inhibition of MraY by protein E. Superposition with previous MraY inhibitor complexes (*26*, *27*) on the YES complex (Fig. 3) shows that the predicted path of the polyisoprenyl chain of C$_{55}$P is the groove formed between TM5 and TM9, which is occluded by protein E. Therefore, one mechanism of inhibition is that protein E prevents access of the lipid substrate to the active site (Fig. 3A). Protein E is a noncompetitive inhibitor of Park's nucleotide (*36*) and, accordingly, the pocket that binds the nucleoside is fully accessible in the present structure (Fig. 3B). Loop 9-10 in MraY contains catalytic histidines that must move toward the binding pocket to facilitate catalysis by completing the active site (*28*). The cytoplasmic helix of protein E separates loop 9-10 from the rest of the active site, blocking this transition and providing a second mechanism of inhibition. Overall, protein E blocks access of the lipid substrate and prevents formation of the active site upon substrate binding.

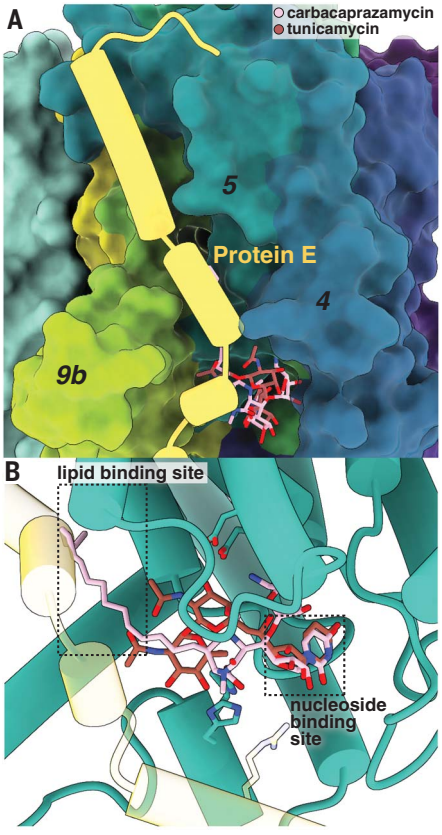

Fig. 3. The mechanism of inhibition by protein E. (**A**) Accessible surface of MraY (colored as in Fig. 2A) viewed from the cytoplasm looking toward the active site cleft. Protein E is shown as an illustration. The structures for the inhibitors tunicamycin (maroon) and carbacaprazamycin (pink) are shown as sticks based on a structural alignment to *Ec*MraY$_A$ with their respective complex structures [PDBID: 6OYH (*26*) and 5JNQ (*27*)]. (**B**) Similar to (A) from a slightly different angle highlighting the catalytic pocket. MraY (dark cyan) is shown as an illustration. The two substrate binding sites are highlighted by dashed boxes. Predicted catalytic residues in MraY are shown as sticks.

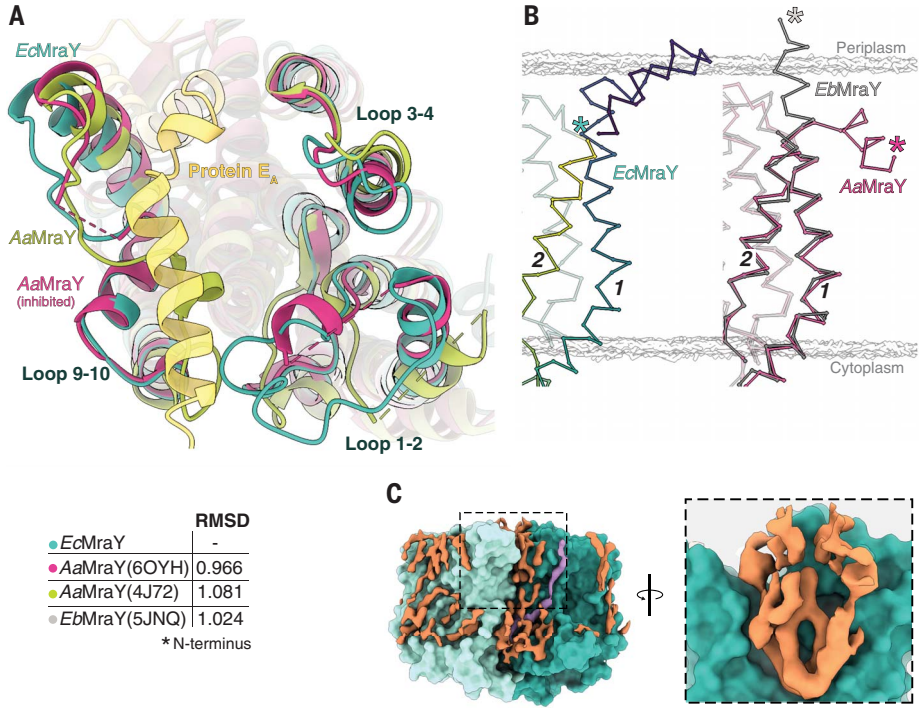

Fig. 4. Features observed in the EM structure of *E. coli* MraY. (**A**) Cytoplasmic view of a structural alignment of *Ec*MraY (dark cyan) against uninhibited *Aa*MraY [green, PDBID:4J72 (*25*)] and carbacaprazamycin inhibited *Aa*MraY [pink, PDBID:6OYH (*26*)]. RMSDs to monomer A of *Ec*MraY are shown. The color scheme for the various MraY crystal structures is used throughout the figures. (**B**) A view in the plane of the membrane showing the region that includes TM1 and TM2 in backbone ribbons. (Left) The *Ec*MraY structure colored from the N terminus through TM2 in the Viridis color scheme. (Right) The inhibited *Aa*MraY structure from (A) and the *Eb*MraY structure [gray, PDBID:5JNQ (*27*)]. Each structure is aligned to *Ec*MraY. The location of each N terminus is indicated by an asterisk. (**C**) Accessible surface of *Ec*MraY (cyan) and unmodeled densities (orange) that are likely lipids or detergent as well as a putative C55P molecule (purple, see below). The inset is a view of the periplasmic cavity viewed from a removed monomer.

Key structural features of MraY

Although there are prior crystallographic MraY structures (*25*–*27*), our YES complex structure reveals *E. coli* MraY in a distinct structural context (fig. S9). There is agreement with the prior structures when comparing MraY monomers with backbone RMSDs around 1 Å (Fig. 4A and fig. S10). We can model previously disordered regions of MraY including all the cytoplasmic loops that enclose the active site. Loop 1-2 likely adopts distinct conformations during the catalytic cycle and indeed has two slightly different conformations in our dimer (fig. S6C). Loop 9-10 adopts a conformation that is similar to the reported small-molecule inhibitor co-crystal structures of MraY (*26*, *27*, *37*) but distinct from the apoprotein structure (Fig. 4 and fig. S10). This conformation of loop 9-10 may be a general feature of MraY complexed with inhibitors.

In prior crystal structures, the N terminus of MraY begins at either TM1 or is a helix that projects away from the structure in an orientation incompatible with the bilayer (Fig. 4B). In the YES complex, the N-terminal end of the first helix (NTH) hydrogen-bonds to the C-terminal end of TM2, effectively forming a helical stacking structure (Fig. 4B and fig. S9C). A multiple sequence alignment across bacteria shows that the NTH in MraY is conserved across gram-negative bacteria but missing in Gram positives (figs. S7 and S11). Although this feature is not found in the crystal structures, AlphaFold (*38*) predicts the NTH stacking for *E. coli* and other Gram-negative bacteria with slight differences in hydrogen bonding and orientation relative to the cryo-EM structure (fig. S11). For the *Aa*MraY structures (*25*, *26*), the positioning of the N terminus is likely a product of crystallization, as AlphaFold predicts the NTH stacks for this and the related *Hydrogenivirga* species (fig. S11). For Gram-positive bacteria, both the *Eb*MraY and predicted structures lack the NTH (*27*) (Fig. 4B and fig. S11).

Protein E as a general antibacterial protein

Expression of protein E leads to lysis that results in a subset of killed bacteria becoming "ghosts"—essentially empty cell walls (*15*). Ghosts have been used in a variety of contexts including vaccine development [reviewed in (*39*)]. For ghosts to be made, protein E must inhibit the native MraY of the target bacteria. Although phage ΦX174 is restricted to *E. coli*, many bacteria have been probed for ghost formation by expression of protein E. All Gram-negative bacteria tested (fig. S11A) resulted in the formation of ghosts [reviewed in (*40*)]. By contrast, protein E was unable to cause lysis in the Gram-positive *Staphylococcus carnosus* (*41*). Expression of the *Bacillus subtilis* MraY in *E. coli* prevented cell lysis, suggesting that it has a low affinity for protein E (*35*). Comparing the residues in *Ec*MraY that contact protein E to those in Gram-positive species, there are no single residue differences that easily explain the inability to inhibit MraY from gram-positive species. There are a few residues that may play a role—such as P170 in *Ec*MraY which confers resistance when mutated to leucine—that are absent in Gram-positive MraYs (fig. S7).

*Ec*MraY residue Y134, which forms a bridge with protein E M26 in our model (Fig. 2C), is also missing in Gram-positive species (fig. S7).

Lipids bound to the YES complex

The YES complex was solubilized from its native environment and, for the YES_{ID21} complex, the final detergent solution was supplemented with *E. coli* lipids. We observe lipid densities around the membrane surface of MraY (Fig. 1D and fig. S12, A and B). Prior work supports a functional role for anionic phospholipids with MraY including stabilizing the dimer (*42*–*44*). We observe substantial lipid density near the dimer interface with features consistent with glycerophospholipids, although not all density can be clearly assigned (fig. S12). As in previous structures (*25*, *27*), there is a hydrophobic periplasmic cavity within the MraY dimer that contains unexplained density (Fig. 4C). Although this density has clear structure, we are unable to fit typical *E. coli* phospholipids.

Recently, a study using native mass spectrometry and molecular dynamics identified a binding site for $C_{55}P$ at the dimer interface with the phosphate headgroup predicted to form a salt bridge to R341 in *Ec*MraY (*44*). In our structure, we observed a long tube of density at the dimer interface (fig. S12A, purple) that ends at R341 and is consistent with $C_{55}P$ (fig. S12C). Although we cannot confidently identify this lipid, the density would be consistent with $C_{55}P$, although the role for this binding site remains to be determined.

The role of SlyD in protein E–mediated lysis

The amphipathic helix of protein E bridges the two *E. coli* proteins, MraY and SlyD, which make no specific contact with each other (Fig. 2A). The IF domain sits on the hydrophobic face of the protein E helix (Fig. 5A) and contacts the extended C terminus of the opposing protein E, which then extends to bind the FKBP domain (Fig. 5B). This results in a bowtie-like interaction with each SlyD binding both protein E–soluble domains (Fig. 1E). There are no contacts between the two SlyD molecules (fig. S6D). These protein E interfaces validate structural studies of SlyD where peptides bind to each of the interfaces seen here including β-augmentation in a groove in the IF domain (Fig. 5, C and D) (*32*). The IF domain binding to an α-helix may be an important chaperoning interaction. The FKBP domain is well-ordered but adopts a range of orientations in our particles (fig. S13) and consequently has the lowest resolution (fig. S3). This flexibility relative to the IF domain is consistent with the NMR structure of SlyD where the orientations of the two domains are not constrained by each other (*31*). The only contact of the FKBP domain to the rest of the YES complex is the flexible linker to the IF domain and binding to the extended C terminus of protein E. We observe continuous backbone density that allows us to place P65 at the FKBP active site. As seen before for some SlyD-bound peptides (*32*), protein E binding to the FKBP domain adopts a noncanonical orientation. Protein E P65 is not completely conserved (fig. S1), although other species have a proline at residue 63 which could reach the active site with additional tilting of the FKBP domain. A proline near this position may help to localize the chaperone to the complex and facilitate assembly.

The lack of contacts between SlyD and MraY suggest that the soluble domain of protein E alone could form a complex with SlyD. We coexpressed *Ec*SlyD with N-terminal truncations of protein E from either ID21 (residues 33 to 76) or the shortest isoform α3 (residues 33 to 75). Both form complexes that could be purified by an affinity tag on the soluble domain (fig. S2E). These observations point to a high-affinity interaction between SlyD and the C-terminal domain of protein E.

Protein E is unstable in the absence of SlyD (*18*) and is rapidly degraded (*23*). It has been speculated that prolyl-isomerization is central to the lysis mechanism (*22*), but this idea is not supported by available evidence. Nonproline mutations in protein E can rescue lysis in a Δ*slyD* background (*18*, *45*), as well as completely replace the cytoplasmic domain of protein E with an unrelated globular protein (*20*, *21*, *45*). We also performed our lysis assay with several SlyD variants in the Δ*slyD* strain (fig. S2C). As before, protein $E_{\Phi X174}$ was unable to promote lysis in the absence of SlyD, however lysis could be rescued by expression of either *Ec*SlyD or $EcSlyD_{154}$. *Thermus thermophilus* (*Tt*) SlyD has high structural homology to *Ec*SlyD (Fig. 5D and fig. S2, B, F, and G) and also rescued lysis in the Δ*slyD* strain (fig. S2C). We generated an *Ec*SlyD Y68K mutant that substantially reduces prolyl-isomerase activity (*46*) and this too could rescue lysis. Finally, we purified a complex of protein E using the Epos rescue mutants (R3H and L19F) (*45*) in the Δ*slyD* strain. This YE complex was very unstable and aggregated according to SEC (fig. S2H). These results support the conclusion that the primary role of SlyD in promoting lysis is not prolyl-isomerization, but to protect protein E and stabilize the YES complex. This does not obviate a role for proline binding in complex assembly. Mutation of P65, in the FKBP active site, creates a slower-lysis phenotype (*22*), which may indicate that binding of these residues by SlyD is key to assembling the YES complex.

Protein E is evolutionarily constrained

Protein E arrived late in the evolution of ΦX174 and was overprinted into a +1 reading frame in the ORF for gene *D* (*47*, *48*). The structure supports that this embedding constrains the evolution of protein E (*12*). Considering the sequence changes across protein E isoforms, we note that from the N terminus through residue 70, with few exceptions, each position that is not completely conserved is either silent or that there is only a slight change in protein D (fig. S8A). The silent changes vary

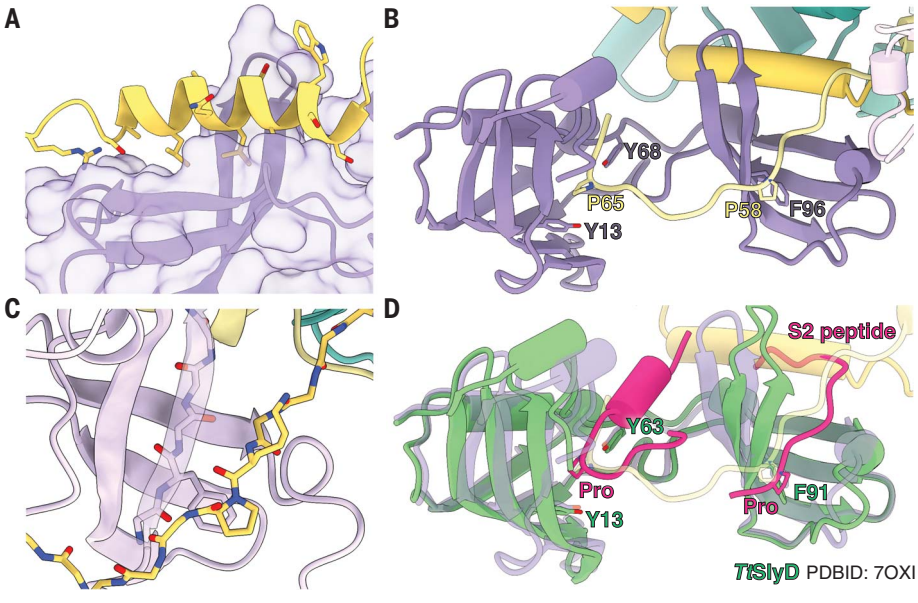

Fig. 5. Interactions between protein E and SlyD. (**A**) The amphipathic helix of protein E (yellow) as a illustration with side chains contacting SlyD shown as sticks. SlyD (purple) is shown as an illustration along with a transparent accessible surface (**B**) Full view of SlyD bound to two protein E molecules shown in different shades of yellow. (**C**) As in (A) highlighting the β-augmentation of the extended C-terminal protein E. (**D**) Structures of SlyD from the YES_{ID21} complex and *Tt*SlyD [PDBID:7OXI (*33*)] (green) aligned to the IF domains. The two S2 peptides bound to the *Tt*SlyD are shown in pink.

the codon's second position, which is the wobble position in the overlapping codon for protein D. For example, residue W7 in ΦX174 is replaced with a Ser or Leu in other species. Although seemingly substantial changes, each is coded by the sequence UXG and all three variations at this position are sampled. These variable positions generally do not contact MraY. An exception is found in the G4 isoform where a phenyalanine occurs at position 19, as in the Epos mutant, which results in a change from alanine to serine at position 79 in protein D. This places a polar residue in the hydrophobic core of protein D (fig. S8). This single nucleotide change increases protein E affinity to MraY but likely lowers the stability of protein D and the overall fitness of the virus. Introduction of this mutation results in smaller plaque formation relative to the wild type (*23*). The C terminus of protein D and the extensions in the longer isoforms of protein E are likely disordered and less constrained, hence the increased sequence variability (fig. S8).

Conclusions

The mechanism for ΦX174 inhibition of peptidoglycan biosynthesis is suprisingly simple. Protein E binds in the active site cleft preventing access of the lipid substrate and blocking conformational changes needed for catalysis (fig. S14). The YES complex structure provides a template for interpreting all the previous results for lysis by ΦX174. Notable among these are that the extensive functional mutations in protein E and MraY map to the interface between the two proteins. SlyD binds to the cytoplasmic domain of protein E to stabilize the MraY/protein E complex. As we demonstrated, the requirement for SlyD is based on the protein binding properties, as distantly related SlyD homologs can rescue lysis in a Δ*slyD* strain. SlyD in this case does not serve directly in the mechanism of inhibition of MraY and can be functionally replaced.

Our structures offer some insights for future work applying SGL proteins as therapies. Protein E binding to *Ec*MraY identifies a distinct mechanism from current inhibitors. Blocking of the lipid substrate access to the active site in MraY could be exploited by small molecules, with structure-based drug design guided by the protein E structure. Expanding protein E efficacy to Gram-positive bacteria and, potentially, other related polyisoprenyl-phosphotransferases such as bacterial WecA or the mammalian DPAGT1 could further increase applicability. SGL proteins, which have distinctly evolved many times (*49*), can also be used to improve the antibacterial potency of bacteriophages. The use of phages for medical therapies, although known for a hundred years, has attracted recent attention (*1*). Improving the efficiency of ΦX174 protein E based on structural information may help these therapies achieve their greatest potential in the fight against antimicrobial-resistant pathogens.

Materials and Methods

Coexpression of EcMraY, protein E, and EcSlyD

Δ*slyD* BL21(DE3)-competent cells were co-transformed with pET22b-SlyD$_{154}$ and either pRSFDuet*Ec*MraY-E$_{ID21}$ or pRSFDuet-*Ec*MraY-E$_{ΦX174}$ and plated in LB-agar containing 35 μg/ml Kanamycin and 100 μg/mL Ampicillin. Our pET22b-SlyD$_{154}$ construct expresses *E. coli* SlyD, modified by the removal of the flexible C-terminus. The pRSFDuet-*Ec*MraY-E$_{ID21}$ plasmid contains the ID21 isoform of protein E, along with a wild-type *Ec*MraY to prevent cell lysis from the overexpression of protein E. Cells were grown in 2xYT media at 37°C, 225 r.p.m., and induced at an OD$_{600}$ of 0.9 with 0.4mM IPTG at 18°C overnight. The culture was harvested by centrifugation for 10 minutes at 9000*xg*, 4°C then frozen or used immediately for purification.

Purification of the YES complex

The cells were resuspended in lysis buffer (20mM Tris-HCl pH 7.5, 300 mM NaCl, 10% Glycerol, 5mM β-mercaptoethanol (βME), 0.1mM PMSF, 0.1mM Benzamidine) and homogenized using a M-110L microfluidizer (Microfluidics). The lysate was cleared by a 20-minute centrifugation at a speed of 22,000*xg*. The supernatant was then centrifugated at 167,424*xg* and the resulting membrane pellet was then solubilized in the extraction buffer [10 mM HEPES pH 7.5, 300 mM NaCl, 5% Glycerol, 5mM βME, 0.1mM phenylmethylsulfonyl fluoride (PMSF), 0.1mM benzamidine, 10 mM imidazole and 1% dodecyl 4-O-α-D-glucopyranosyl-β-D-glucopyranoside (DDM)] After allowing for extraction for 1.5 hours at 4°C, the solution was centrifuged at 167,424*xg* for 30 minutes and the remaining lysate was mixed with 1mL NiNTA resin (Qiagen, Alameda, CA) then nutated at 4°C for two hours. This solution was loaded onto a gravity column and then washed with five column volumes of wash buffer (10 mM HEPES pH 7.5, 150 mM NaCl, 5% glycerol, 5mM βME, & 0.03% DDM) with 10mM imidazole followed by five column volumes of wash buffer with 30 mM imidazole. The YES complex was eluted in 20mL of wash buffer containing 200 mM imidazole. The final purification step was SEC (Superdex 200 10/300 GL, Millipore Sigma) in 10mM HEPES pH 7.5, 75 mM NaCl, 5% Glycerol, 5mM βME and 0.03% DDM. Fractions were assessed by SDS-PAGE and directly used for cryo-EM sample preparation.

Co-expression of EcMraY and protein E in various SlyD backgrounds

The pRSFDuet-E-*Ec*MraY and pRSFDuet-Epos-*Ec*MraY expression vectors were transformed into BL21-Star cells (Novagen). Similarly, the pRSFDuet-E(C-term)-SlyD$_{154}$ was transformed into SlyD-knockout cells. The cultures were grown at 37 °C to an OD$_{600}$ 0.8 and induced with 1 mM IPTG. Induced cultures were grown for 3 hours followed by harvesting by centrifugation at 9,000*xg* for 20 min. Cell pellets were resuspended in lysis buffer and lysed by sonication. The lysate was then cleared by centrifugation at 22,000*xg*, followed by a second centrifugation at 234,78*xg* for 1 hour to isolate the membrane fraction. The complex was extracted in 20 mM Tris-HCl pH 7.5, 300 mM NaCl, 10% Glycerol, 10 mM Imidazole, and 1% n-Decyl-β-Maltoside (DM) and incubated at 4°C for 1.5 hours. The debris was cleared by centrifugation at 234,788*xg* for 30 min. The sample was incubated with 1 mL NiNTA resin for 1 hour, followed by a wash with 50 column volumes lysis buffer with 30mM Imidazole. The protein E complexes were similarly eluted in 300mM Imidazole. The elutions were concentrated and further purified by size exclusion chromatography (Superdex 200 10/300 GL, Millipore Sigma).

Lysis assays of WT protein E ΦX174 and ID21

LEMO DE3 competent cells were transformed with a pRSF-Duet vector either empty, with protein E$_{ΦX174}$, or protein E$_{ID21}$. Cultures were grown to an OD$_{600}$ of 0.2 and inoculated into a Corning 96-well Clear Flat Bottom plates in 100μL triplicate aliquots and induced as described previously. Cultures were incubated at 37C with orbital shaking at 220rpm using an Infinite M Nano+ (Tecan, Switzerland). Readings were taken in 5-minute intervals for 90 minutes.

Lysis assay for protein E constructs

LEMO DE3 competent cells (New England Biolabs, MA, USA) were transformed with a pRSFDuet vector either empty, with C-terminally FLAG tagged protein E$_{ΦX174}$ variants (WT, P21A, K46A). The lysis assays were performed in three biological replicates as previously described (*21*). Absorbance readings were recorded in 5-minute intervals for 1 hour and 30 minutes. Manual readings were taken using a Biowave Cell Density Meter CO8000. The values were plotted using GraphPad Prism version 9.1.1 for macOS.

Lysis assays based on SlyD variants

Δ*slyD* (*18*) cells were transformed with either a control empty pRSF-Duet vector or pRSFDuet-Protein$_{ΦX174}$ and either pET22b-*Ec*SlyD, pET22b-SlyD$_{154}$, pET22b-*Ec*SlyD Y68K, or pET22b-*Thermus thermophilus* SlyD. Cultures were grown in 2xYT media at 37°C and induced with 0.4mM IPTG once at an OD$_{600}$ of 0.2. Absorbance measurements were manually recorded in 5-minute intervals for 70 minutes. Similarly, Δ*slyD* cells were transformed with either a control empty pRSF-Duet vector or pRSF-Duet-Protein$_{ID21}$ either alone, with pET22b*Ec*SlyD, or with pET22b-*Ec*SlyD$_{154}$ and induced with 0.4mM IPTG. Readings were recorded using an Infinite M Nano+ plate reader as described above.

Sample preparation for cryoEM

The YES complex was diluted to 5.0 mg/mL in 10 mM HEPES pH 7.5, 75 mM NaCl, 5% Glycerol, 5mM βME and 0.03% DDM. Additionally, the YES_{ID21} sample was supplemented with 1mM *E. coli* total lipid extract (Avanti Polar Lipids, 100600P). Quantifoil holey carbon films R1.2/1.3 300 Mesh, Copper (Quantifoil, Micro Tools GmbH) grids were glow discharged with a 2-minute 20Å plasma current using a Pelco easiGlow, Emitech K100X. Grids were prepared using a Vitrobot (FEI Vitrobot Mark v4 x2, Mark v3) by applying 3μL of sample onto the grid followed by a 3.5 second blot using a +8-blot force and plunge frozen into liquid ethane.

Data acquisition and analysis

The grids were imaged in a 300 kV cryo-TEM microscope equipped with a Gatan K3 6k x 4k direct electron detector and a Gatan Energy Filter (slit width 20eV) in super-resolution mode using Serial EM. Datasets were collected at a 105k magnification with a pixel size of 0.416 Å/pixel. Movies with 40 frames were recorded with a total exposure dose of 60 $e^-/Å^2$ and a defocus range of -1.0 to -2.5 μm. For the YES_{ID21} complex, a total of 12,070 movies were recorded. Movies were normalized by gain reference and motion corrected using the patch motion correction built in function in cryosparc (v3.3.2) with a twofold bin that resulted in a pixel size of 0.832 Å/pixel (*50*). The contrast transfer function (CTF) was estimated using CTFFIND4 (*51*). Micrographs were manually curated, and low-quality images were removed for further analyses. A total of 2,462,335 particles were obtained followed by the generation of 6 ab-initio models. Out of the 6 models, two models are selected for classification into "good" and "trash" volumes. All particles were then sorted in these two volumes through heterogeneous refinement using particles extracted with a 4x bin, which produced 6,589,696 good particles. Heterogeneous refinement was used in an iterative manner to sort the particles into the 5 volumes (4 good and 1 trash). The 1,151,777 good particles were used for non-uniform homogeneous refinement to generate a higher resolution volume. The particles were then extracted with a 3x bin and sorted into 4 iterations of the higher resolution volume and 1 trash volume. Iterative rounds of heterogeneous refinement at 3x bin produced 935,754 particles. Particles were then extracted in a 2x bin and heterogeneously refined into either high- or low-resolution volumes. At this point, discerning features in the soluble region of the model were used to select the most complete volumes. The volumes were individually refined through non-uniform refinement and the particles that composed the volumes with most complete and highest resolution were used. A total of 122,452 particles were used for the most complete model obtained upon non-uniform refinement. The FSC-masked resolution was 3.5Å, while the unmasked resolution was 3.9Å. The half-maps were then used for post-processing through DeepEMhancer (*52*) with the high-resolution model selected for our most complete density map. Post-processing through DeepEMhancer removed the micelle and improved the features on the soluble portions of the map, however the lipid densities were also removed. The lipid densities described in this work are those of the YES_{ID21} map before post-processing. Notably, the dimer-interface lipid density was also present in the $YES_{ΦX174}$ density map without the supplementation of *E. coli* lipid extract. Figure 1D uses the densities before post-processing for the MraY dimer, micelle and lipid densities, and the DeepEMhancer post-processed map for protein E and SlyD. Supplemental figures S9 and S12 were made with the map before DeepEMhancer sharpening. The $YES_{ΦX174}$ complex dataset was processed in this same manner. A total of 10,798 movies were recorded. The model for the YES_{ID21} complex was then used as a template for template picking, from which 1,516,368 particles were picked and curated. Following gradual un-binning and sorting into good and trash volumes, 155,270 particles were used for the final iteration of non-uniform refinement. The local resolution of both maps was performed on cryosparc (v3.3.2). The half-maps were then post-processed using DeepEMhancer as described previously.

Model building

For starting models we used the *Aquifex aeolicus* un-bound structure (PDBID:4J72) (*25*) for *Ec*MraY and the *E. coli* NMR structure (PDBID:2K8I) (*31*) for *Ec*SlyD which were fit using phenix.dock. SlyD was then split into its two domains, IF and FKBP, at residues Y68 and G127. Protein E was modeled de novo up to residue P65 using Coot 0.8.9.2. The structures of the *Ec*MraY, protein E, and *Ec*SlyD-IF domain were refined using phenix.real space refinement and ISOLDE 1.6, and validated with PHENIX-1.19.2. After the refinements of *Ec*MraY, protein E, and the *Ec*SlyD-IF domain were completed, the FKBP domains were docked into density using ChimeraX. The complete YES complex structure was then refined using PHENIX-1.19.2 and ISOLDE 1.6. RMSDs were calculated using ChimeraX Matchmaker chain alignment. Structure figures were made using ChimeraX and sequence alignments using Jalview and ClustalW (*53–55*).

REFERENCES AND NOTES

1. S. A. Strathdee, G. F. Hatfull, V. K. Mutalik, R. T. Schooley, Phage therapy: From biological mechanisms to future directions. *Cell* **186**, 17–31 (2023). doi: 10.1016/j.cell.2022.11.017; pmid: 36608652
2. R. T. Schooley *et al*., Development and Use of Personalized Bacteriophage-Based Therapeutic Cocktails To Treat a Patient with a Disseminated Resistant *Acinetobacter baumannii* Infection. *Antimicrob. Agents Chemother.* **61**, e00954–e17 (2017). doi: 10.1128/AAC.00954-17; pmid: 28807909
3. C. Ferriol-González, P. Domingo-Calap, Phage Therapy in Livestock and Companion Animals. *Antibiotics* **10**, 559 (2021). doi: 10.3390/antibiotics10050559; pmid: 34064754
4. K. E. Kortright, B. K. Chan, J. L. Koff, P. E. Turner, Phage therapy: A renewed approach to combat antibiotic-resistant bacteria. *Cell Host Microbe* **25**, 219–232 (2019). doi: 10.1016/j.chom.2019.01.014; pmid: 30763536
5. F. D. Herelle, [The bacteriophage]. *Atomes* **3**, 399–403 (1948). pmid: 18104413
6. R. L. Sinsheimer, A single-stranded deoxyribonucleic acid from bacteriophage ΦX174. *J. Mol. Biol.* **1**, 43–IN6 (1959). doi: 10.1016/S0022-2836(59)80006-1
7. C. A. Hutchison 3rd, R. L. Sinsheimer, The process of infection with bacteriophage phi-X174: X. Mutations in a phi-X Lysis gene. *J. Mol. Biol.* **18**, 429–447 (1966). doi: 10.1016/S0022-2836(66)80035-9; pmid: 5968177
8. R. M. Benbow, C. A. HutchisonIII, J. D. Fabricant, R. L. Sinsheimer, Genetic map of bacteriophage ΦX174. *J. Virol.* **7**, 549–558 (1971). doi: 10.1128/jvi.7.5.549-558.1971; pmid: 16789129
9. H. O. Smith, C. A. Hutchison3rd, C. Pfannkoch, J. C. Venter, Generating a synthetic genome by whole genome assembly: phiX174 bacteriophage from synthetic oligonucleotides. *Proc. Natl. Acad. Sci. U.S.A.* **100**, 15440–15445 (2003). doi: 10.1073/pnas.2237126100; pmid: 14657399
10. M.-S. Kim, E.-J. Park, S. W. Roh, J.-W. Bae, Diversity and abundance of single-stranded DNA viruses in human feces. *Appl. Environ. Microbiol.* **77**, 8062–8070 (2011). doi: 10.1128/AEM.06331-11; pmid: 21948823
11. F. Sanger *et al*., Nucleotide sequence of bacteriophage phi X174 DNA. *Nature* **265**, 687–695 (1977). doi: 10.1038/265687a0; pmid: 870828
12. B. G. Barrell, G. M. Air, C. A. Hutchison 3rd, Overlapping genes in bacteriophage phiX174. *Nature* **264**, 34–41 (1976). doi: 10.1038/264034a0; pmid: 1004533
13. K. D. Young, R. Young, Lytic action of cloned phi X174 gene E. *J. Virol.* **44**, 993–1002 (1982). doi: 10.1128/jvi.44.3.993-1002.1982; pmid: 6294347
14. W. Lubitz, G. Halfmann, R. Plapp, Lysis of Escherichia coli after infection with phiX174 depends on the regulation of the cellular autolytic system. *J. Gen. Microbiol.* **130**, 1079–1087 (1984). doi: 10.1099/00221287-130-5-1079; pmid: 6236279
15. A. Witte, G. Wanner, M. Sulzner, W. Lubitz, Dynamics of PhiX174 protein E-mediated lysis of Escherichia coli. *Arch. Microbiol.* **157**, 381–388 (1992). doi: 10.1007/BF00248685; pmid: 1534215
16. T. G. Bernhardt, W. D. Roof, R. Young, Genetic evidence that the bacteriophage phi X174 lysis protein inhibits cell wall synthesis. *Proc. Natl. Acad. Sci. U.S.A.* **97**, 4297–4302 (2000). doi: 10.1073/pnas.97.8.4297; pmid: 10760296
17. D. Maratea, K. Young, R. Young, Deletion and fusion analysis of the phage phi X174 lysis gene E. *Gene* **40**, 39–46 (1985). doi: 10.1016/0378-1119(85)90022-8; pmid: 2936651
18. W. D. Roof, S. M. Horne, K. D. Young, R. Young, slyD, a host gene required for phi X174 lysis, is related to the FK506-binding protein family of peptidyl-prolyl cis-trans-isomerases. *J. Biol. Chem.* **269**, 2902–2910 (1994). doi: 10.1016/S0021-9258(17)42027-8; pmid: 8300625
19. K. R. Chamakura, R. Young, Single-gene lysis in the metagenomic era. *Curr. Opin. Microbiol.* **56**, 109–117 (2020). doi: 10.1016/j.mib.2020.09.015; pmid: 33075663
20. K. J. Buckley, M. Hayashi, Lytic activity localized to membrane-spanning region of phi X174 E protein. *Mol. Gen. Genet.* **204**, 120–125 (1986). doi: 10.1007/BF00330198; pmid: 3018438
21. S. Tanaka, W. M. Clemons Jr., Minimal requirements for inhibition of MraY by lysis protein E from bacteriophage ΦX174. *Mol. Microbiol.* **85**, 975–985 (2012). doi: 10.1111/j.1365-2958.2012.08153.x; pmid: 22742425
22. A. Witte, G. Schrot, P. Schön, W. Lubitz, Proline 21, a residue within the α-helical domain of phiX174 lysis protein E, is required for its function in Escherichia coli. *Mol. Microbiol.* **26**, 337–346 (2003). doi: 10.1046/j.1365-2958.1997.5781941.x; pmid: 9383158
23. T. G. Bernhardt, W. D. Roof, R. Young, The Escherichia coli FKBP-type PPIase SlyD is required for the stabilization of the E lysis protein of bacteriophage φ X174. *Mol. Microbiol.* **45**, 99–108 (2002). doi: 10.1046/j.1365-2958.2002.02984.x; pmid: 12100551
24. A. C. Teo, D. I. Roper, Core steps of membrane-bound peptidoglycan biosynthesis: Recent advances, insight and opportunities. *Antibiotics* **4**, 495–520 (2015). doi: 10.3390/antibiotics4040495; pmid: 27025638
25. B. C. Chung *et al*., Crystal structure of MraY, an essential membrane enzyme for bacterial cell wall synthesis. *Science*

341, 1012–1016 (2013). doi: 10.1126/science.1236501; pmid: 23990562
26. E. H. Mashalidis *et al*., Chemical logic of MraY inhibition by antibacterial nucleoside natural products. *Nat. Commun.* **10**, 2917 (2019). doi: 10.1038/s41467-019-10957-9; pmid: 31266949
27. J. K. Hakulinen *et al*., MraY-antibiotic complex reveals details of tunicamycin mode of action. *Nat. Chem. Biol.* **13**, 265–267 (2017). doi: 10.1038/nchembio.2270; pmid: 28068312
28. B. Al-Dabbagh *et al*., Active site mapping of MraY, a member of the polyprenyl-phosphate N-acetylhexosamine 1-phosphate transferase superfamily, catalyzing the first membrane step of peptidoglycan biosynthesis. *Biochemistry* **47**, 8919–8928 (2008). doi: 10.1021/bi8006274; pmid: 18672909
29. V. V. Mokhonov *et al*., SlyD-deficient *Escherichia coli* strains: A highway to contaminant-free protein extraction. *Biochem. Biophys. Res. Commun.* **499**, 967–972 (2018). doi: 10.1016/j.bbrc.2018.04.029; pmid: 29626483
30. C. Löw *et al*., Crystal structure determination and functional characterization of the metallochaperone SlyD from *Thermus thermophilus*. *J. Mol. Biol.* **398**, 375–390 (2010). doi: 10.1016/j.jmb.2010.03.014; pmid: 20230833
31. U. Weininger *et al*., NMR solution structure of SlyD from Escherichia coli: Spatial separation of prolyl isomerase and chaperone function. *J. Mol. Biol.* **387**, 295–305 (2009). doi: 10.1016/j.jmb.2009.01.034; pmid: 19356587
32. E. M. Quistgaard *et al*., Molecular insights into substrate recognition and catalytic mechanism of the chaperone and FKBP peptidyl-prolyl isomerase SlyD. *BMC Biol.* **14**, 82 (2016). doi: 10.1186/s12915-016-0300-3; pmid: 27664121
33. S. Pazicky, A. A. Werle, J. Lei, C. Löw, U. Weininger, Impact of distant peptide substrate residues on enzymatic activity of SlyD. *Cell. Mol. Life Sci.* **79**, 138 (2022). doi: 10.1007/s00018-022-04179-4; pmid: 35184231
34. L. Martino *et al*., The interaction of the *Escherichia coli* protein SlyD with nickel ions illuminates the mechanism of regulation of its peptidyl-prolyl isomerase activity. *FEBS J.* **276**, 4529–4544 (2009). doi: 10.1111/j.1742-4658.2009.07159.x; pmid: 19645725
35. Y. Zheng, D. K. Struck, T. G. Bernhardt, R. Young, Genetic analysis of MraY inhibition by the phiX174 protein E. *Genetics* **180**, 1459–1466 (2008). doi: 10.1534/genetics.108.093443; pmid: 18791230
36. Y. Zheng, D. K. Struck, R. Young, Purification and functional characterization of phiX174 lysis protein E. *Biochemistry* **48**, 4999–5006 (2009). doi: 10.1021/bi900469g; pmid: 19379010
37. B. C. Chung *et al*., Structural insights into inhibition of lipid I production in bacterial cell wall synthesis. *Nature* **533**, 557–560 (2016). doi: 10.1038/nature17636; pmid: 27088606
38. J. Jumper *et al*., Highly accurate protein structure prediction with AlphaFold. *Nature* **596**, 583–589 (2021). doi: 10.1038/s41586-021-03819-2; pmid: 34265844
39. P. Kudela, V. J. Koller, W. Lubitz, Bacterial ghosts (BGs)—Advanced antigen and drug delivery system. *Vaccine* **28**, 5760–5767 (2010). doi: 10.1016/j.vaccine.2010.06.087; pmid: 20619379
40. U. B. Mayr *et al*., Bacterial ghosts as antigen delivery vehicles. *Adv. Drug Deliv. Rev.* **57**, 1381–1391 (2005). doi: 10.1016/j.addr.2005.01.027; pmid: 15878634
41. G. Halfmann, F. Götz, W. Lubitz, Expression of bacteriophage PhiX174 lysis gene E in Staphylococcus carnosus TM300. *FEMS Microbiol. Lett.* **108**, 139–143 (1993). doi: 10.1111/j.1574-6968.1993.tb06089.x; pmid: 8486239
42. E. Henrich *et al*., Lipid Requirements for the Enzymatic Activity of MraY Translocases and in Vitro Reconstitution of the Lipid II Synthesis Pathway. *J. Biol. Chem.* **291**, 2535–2546 (2016). doi: 10.1074/jbc.M115.664292; pmid: 26620564
43. E. Henrich *et al*., Analyzing native membrane protein assembly in nanodiscs by combined non-covalent mass spectrometry and synthetic biology. *eLife* **6**, e20954 (2017). doi: 10.7554/eLife.20954; pmid: 28067619
44. A. O. Oluwole *et al*., Peptidoglycan biosynthesis is driven by lipid transfer along enzyme-substrate affinity gradients. *Nat. Commun.* **13**, 2278 (2022). doi: 10.1038/s41467-022-29836-x; pmid: 35477938
45. W. D. Roof, R. Young, Φ X174 lysis requires slyD, a host gene which is related to the FKBP family of peptidyl-prolyl cis-trans isomerases. *FEMS Microbiol. Rev.* **17**, 213–218 (1995). doi: 10.1016/0168-6445(94)00073-5; pmid: 7669348
46. T. Ikura, N. Ito, Requirements for peptidyl-prolyl isomerization activity: A comprehensive mutational analysis of the substrate-binding cavity of FK506-binding protein 12. *Protein Sci.* **16**, 2618–2625 (2007). doi: 10.1110/ps.073203707; pmid: 18029417
47. J. C. Fiddes, G. N. Godson, Evolution of the three overlapping gene systems in G4 and phi X174. *J. Mol. Biol.* **133**, 19–43 (1979). doi: 10.1016/0022-2836(79)90249-3; pmid: 160951
48. A. Pavesi, Origin, evolution and stability of overlapping genes in viruses: A systematic review. *Genes* **12**, 809 (2021). doi: 10.3390/genes12060809; pmid: 34073395
49. K. R. Chamakura *et al*., Rapid de novo evolution of lysis genes in single-stranded RNA phages. *Nat. Commun.* **11**, 6009 (2020). doi: 10.1038/s41467-020-19860-0; pmid: 33243984
50. A. Punjani, J. L. Rubinstein, D. J. Fleet, M. A. Brubaker, cryoSPARC: Algorithms for rapid unsupervised cryo-EM structure determination. *Nat. Methods* **14**, 290–296 (2017). doi: 10.1038/nmeth.4169; pmid: 28165473
51. A. Rohou, N. Grigorieff, CTFFIND4: Fast and accurate defocus estimation from electron micrographs. *J. Struct. Biol.* **192**, 216–221 (2015). doi: 10.1016/j.jsb.2015.08.008; pmid: 26278980
52. R. Sanchez-Garcia *et al*., DeepEMhancer: A deep learning solution for cryo-EM volume post-processing. *Commun. Biol.* **4**, 874 (2021). doi: 10.1038/s42003-021-02399-1; pmid: 34267316
53. E. F. Pettersen *et al*., UCSF ChimeraX: Structure visualization for researchers, educators, and developers. *Protein Sci.* **30**, 70–82 (2021). doi: 10.1002/pro.3943; pmid: 32881101
54. A. M. Waterhouse, J. B. Procter, D. M. Martin, M. Clamp, G. J. Barton, Jalview Version 2—A multiple sequence alignment editor and analysis workbench. *Bioinformatics* **25**, 1189–1191 (2009). doi: 10.1093/bioinformatics/btp033; pmid: 19151095
55. M. Steinegger, J. Söding, Clustering huge protein sequence sets in linear time. *Nat. Commun.* **9**, 2542 (2018). doi: 10.1038/s41467-018-04964-5; pmid: 29959318

ACKNOWLEDGMENTS

We are particularly grateful to R. Young and T. Bernhardt for providing inspiration and feedback during the course of this project. We thank them, M. Kurosu, and D. Rees for critical feedback on the manuscript. We further thank R. Young for providing the Δ*slyD* strain. (Cryo) Electron microscopy was done in the Beckman Institute Resource Center for Transmission Electron Microscopy at Caltech. We are grateful to S. Chen for help with data collection and processing. **Funding:** This work was funded by the following: National Institutes of Health grant R01GM114611 (to W.M.C. and M.K.); National Institutes of Health grant DP1GM105385 (to W.M.C.); and the G. Harold and Leila Y. Mathers Foundation (to W.M.C.) **Author contributions:** Conceptualization: S.T. and W.M.C. Methodology: A.K.O., N.R., Y.E.L., S.T., H.G.Y., L.K., and W.M.C. Investigation: A.K.O., N.R., Y.E.L., S.T., H.G.Y., L.K., W.M.C. Visualization: A.K.O., N.R., S.T., and W.M.C. Funding acquisition: W.M.C. Project administration: W.M.C. Supervision: W.M.C. Writing – original draft: A.K.O., N.R., and W.M.C. Writing – review and editing: A.K.O., N.R., Y.E.L., S.T., H.G.Y., L.K., and W.M.C. **Competing interests:** Authors declare that they have no competing interests. **Data and materials availability:** All experimental data are available in the main text or the supplementary materials. Coordinates with experimental maps have been deposited to the RCSB or the EMDB for both the YES_{ID21} (PDB ID 8G01, EMDB-29641) and $YES_{\Phi X174}$ (PDB ID 8G02 and EMDB-29642) complexes.

SUPPLEMENTARY MATERIALS

science.org/doi/10.1126/science.adg9091
Figs. S1 to S14
Table S1
References (*56*–*57*)
MDAR Reproducibility Checklist
Movie S1

View/request a protocol for this paper from *Bio-protocol*.

Submitted 4 February 2023; accepted 23 May 2023
10.1126/science.adg9091